Modeling and Simulation of Asteroid Retrieval Using a Flexible Capture Mechanism

Håvard Fjær Grip, Masahiro Ono,
J. Balaram, Jonathan Cameron, Abhinandan Jain, Calvin Kuo, Steven Myint, Marco Quadrelli

NASA Jet Propulsion Laboratory
California Institute of Technology
4800 Oak Grove Dr.
Pasadena, CA 91109

***Abstract*—The National Aeronautics and Space Administration is currently considering an *Asteroid Redirect Mission* (ARM), the goal of which is to bring a near-Earth asteroid into lunar orbit for inspection by a team of human astronauts. In this paper we present the results of a simulation study that focuses on the challenge of capturing a target asteroid using a robotic spacecraft. This simulation study was conducted in parallel with an ongoing mechanical design process, with the goal of providing feedback on specific design concepts, deriving high-level design targets via optimization, and exploring the trade space of the capture problem independently. We present and discuss several simulation models, the results of which have influenced the evolution of the ARM project to date.**

TABLE OF CONTENTS

1. INTRODUCTION

The National Aeronautics and Space Administration (NASA) is currently considering the possibility of an *Asteroid Redirect Mission* (ARM), the goal of which is to bring a small near-Earth asteroid (NEA) into lunar orbit for inspection by a team of human astronauts. A robotic *Asteroid Retrieval Vehicle* (ARV) would be responsible for capturing the asteroid—measuring up to 13 m in diameter with a mass of up to $1,000,000$ kg—and bringing it into lunar orbit, while a separately launched crew vehicle would carry the astronauts to and from the asteroid. The Asteroid Redirect Mission would enhance our understanding of NEAs, demonstrate new technologies, and lay the groundwork for future missions, for purposes such as resource mining and planetary defense.

The ARV must be capable of rendezvousing with, capturing, and de-spinning the target asteroid before transporting it into lunar orbit. This process is subject to significant uncertainties related to the composition, shape, and mass of the asteroid. A further complicating factor is the spin state of the asteroid: it is likely to be tumbling rather than spinning about a well-defined axis, and may exhibit instantaneous spin rates of as much as 2 RPM. The design of a capture system that is robust against these uncertainties is a challenging task involving a number of competing demands and tradeoffs in the areas of mechanical design and guidance, navigation, and control.

While the capture system could be constructed in a number of different ways, a study by the Keck Institute for Space Studies at Caltech [1] concluded that the most promising design is a flexible bagging mechanism attached to the spacecraft, which would fully envelop and cinch down on the asteroid. Such a mechanism would be suitable both for a solid rock and a rubble pile, and would thus ensure robustness against uncertainty in the asteroid composition. The complex motion of the asteroid places high demands on the capture mechanism, which is responsible for maintaining adequate separation between the asteroid and the spacecraft throughout the capture event, while also cushioning the spacecraft against excessive loads. Of particular concern in this context are the solar array drive assemblies (SADAs), which are expected to tolerate a maximum bending moment equivalent to an acceleration of approximately 0.1 g at the middle of each deployed solar panel.

Topics of This Paper

In this paper we describe the results of a simulation study into the dynamics of an asteroid capture event. This study has been conducted in parallel with an ongoing mechanical design process at NASA's Jet Propulsion Laboratory (JPL), with the goal of providing feedback on specific design concepts, deriving target design parameters via optimization, and exploring the trade space of the capture problem independently.

The simulation team worked closely with the mechanical design team that was responsible for developing the capture mechanism. Since the device was new and quite unlike that in any conventional spacecraft or robotic device, both teams were forced into exploratory spirals of concept development and feasibility assessment, with the results from each team informing the activities of the other. The teams also had to develop and refine the methodologies associated with the design process itself, such as defining the appropriate performance metrics to design to and monitor in the simulation (e.g., monitoring key structural loads and geometric clearances), determining the level of simulation fidelity that was most appropriate for a design at a particular level of maturity (e.g., the modeling of the compliance provided by the capture device as a generalized spring-damper system), establishing the kinds of information that needed to be exchanged between the teams (e.g., mathematical abstractions of specific bag-

to-line friction interactions or pneumatic structure stiffness), and specifying the cross-validation that was necessary at each step of the process (e.g., comparing the simulation loads for a capture scenario that was particularly simple and therefore amenable to being modeled in a tool such as *Adams*).

Background and Capture Phases—We begin in Section 2 by presenting some basic background information on the rotational dynamics of rigid objects in general and NEAs in particular. In Section 3 we summarize the different phases of the capture problem and address the topic of how to approach a tumbling asteroid in preparation for capture. Although it is theoretically possible for a spacecraft equipped with sufficiently large thrusters to match the tumbling motion of the asteroid, such a solution is not considered feasible because of the associated fuel requirements. Thus, it is instead assumed that the spacecraft will approach the asteroid along a well-defined inertial vector while spinning about its symmetry axis, and that the capture event itself is passive from a GN&C standpoint. The choice of approach vector, spin rate, and capture epoch all have major influences on the transient dynamics of the capture event and the eventual steady-state motion regime of the combined spacecraft-asteroid system.

Simulation models—Due to the many unique and unexplored aspects of the asteroid capture problem, some of the trades involved in designing a viable capture system have only become apparent in the course of the simulation study. Our presentation in this paper mirrors the evolving nature of the work that has been conducted, in that we study several different models with different objectives in mind.

In Section 4 we focus on a model representing a design in which robotic limbs extend from the spacecraft bus to form a large barrel. A drawstring bag inside this barrel is attached to the limbs via flexible winch-controlled cinch lines. A central idea of this design is that, after the initial short-duration cinching event, enough flexibility should be left in the system to facilitate passive damping of the tumbling motion toward major-axis spin. This design concept, which we refer to as the *spider-web* capture mechanism, was abandoned due to mechanical design and packaging considerations; however, we discuss it here for the sake of completeness.

In Section 5 we focus on a model created as a rough representation of an alternative design, where the robotic limbs have been replaced by an inflatable exoskeleton attached directly to the spacecraft bus. In this design, the bag collapses around the asteroid with the help of actively controlled winches, while additional inflatable members help keep the spacecraft and the asteroid separated.

In Section 6 we focus on a model that does not represent a particular design, but rather an abstract representation of a capture mechanism with an isolation device represented by a 6-DOF joint. This model allows us to explore, in a general way, the requirements that must be imposed on such an isolation device in order to ensure robustness against various uncertainties.

Each of the three simulation models is based on the same basic building blocks of rigid bodies connected via translational and rotational spring-dampers. The result is clearly a simplification of a complex physical system; we stress, however, that the goal here is not to investigate specific designs at a detail level, but to gain a high-level understanding of the interplay between various factors such as capture geometry, flexibility and damping of the capture mechanism, the tumbling motion of the asteroid, and the relative state of the spacecraft at the time of capture.

Implementation—The simulations were based on the Darts/D-shell architecture for spacecraft dynamics simulation, developed at JPL (see, e.g., [2]). In addition to point simulations for particular configurations, large-scale parametric sweeps were conducted to cover a wide range of asteroid masses, shapes, and rotational states. Moreover, the simulation models were used as components of an optimization algorithm in order to synthesize a set of desirable parameters for a capture mechanism. These topics are discussed in Sections 7 and 8.

2. BACKGROUND

For a rigid body subject to no external torques, the angular velocity $\omega \in \mathbb{R}^3$ around the center of mass (decomposed in body-fixed coordinates) is governed by the *Euler equations*

$$J\dot{\omega} = -\omega \times J\omega, \tag{1}$$

where J is the inertia around the center of mass. By aligning the body-fixed frame with the *principal axes* of the body, the inertia matrix can be written as $J = \mathrm{diag}(I_1, I_2, I_3)$, where I_1, I_2, and I_3 are the principal-axis inertias. From (1) it is easy to see that ω is constant if and only if ω and $J\omega$ are parallel. This is always the case when the principal-axis inertias are identical, but in general ω remains constant only if it is aligned with one of the principal axes. When this is not the case, both the direction and magnitude of ω may vary over time, and the body is said to *tumble*.

A body with three distinct inertias is called a *tri-inertial* body, whereas a body with two identical inertias is called an *inertially axi-symmetrical* body. For tri-inertial bodies, the analytical solution of (1) follows elliptical curves that lie on the surface of two ellipsoids defined by the requirements that the kinetic energy and the angular momentum of the system are both preserved. For axi-symmetrical bodies, the motion can be more conveniently described by representing the attitude using Euler angles labeled *precession*, *nutation*, and *spin*, of which the nutation angle remains constant and the precession and spin angles change at constant rates.

If the rotating body is augmented with damped flexible modes, then these will tend to be excited by the tumbling motion, resulting in a loss of rotational energy. This energy loss eventually leads to convergence toward constant spin around the principal axis with the largest inertia (i.e., major-axis spin). For further details, see [3].

Near-Earth Asteroids

Due to the energy loss associated with flexible modes, celestial objects tend to stabilize toward major-axis spin over time. The relaxation (or characteristic) time, defined as the time required for a tumbling object to achieve a principal axis spin, for an asteroid of radius r and spin period T, is proportional to T^3 and inversely proportional to r^2 [4]. Thus, slow rotating spinners take a long time to achieve principal axis spin, as do small asteroids. For small objects such as near-Earth asteroids in the 10-m class, the convergence is thought to occur on a significantly longer time scale than the average time since last collision. Consequently, it is expected that the ARM target asteroid may tumble.

The instantaneous spin rates for large objects is bounded by the *rubble pile limit* spin barrier at which centrifugal forces

disaggregate bodies composed of a loose collection of smaller objects (i.e., rubble) held together by gravity. Smaller objects, being more solid, are not constrained by this limit, and at the extreme end are seen to approach or slightly exceed spin rates of as much as 2 RPM. We therefore take 2 RPM, un-relaxed objects as the design point for our analysis and simulations. For a number of bounding analysis cases, we consider simply nutated axi-symmetrical bodies; however, we also consider fully tumbling tri-inertial objects.

Coordinate Frames

In each of the simulations presented in this paper, the initial angular momentum vector of the asteroid is aligned with the z axis of the inertial reference coordinate frame. When discussing inertially axi-symmetrical asteroids, we align the symmetry axis with the asteroid's z axis; for tri-inertial asteroids (modeled as ellipsoids), we align the smallest semi-axis with the z axis. We define the axes of the spacecraft according the convention illustrated in Figure 1.

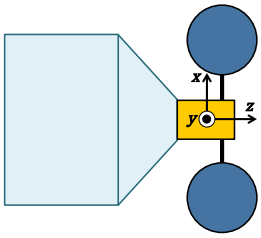

Figure 1. Spacecraft axes convention

3. CAPTURE PHASES

The asteroid capture problem is composed of the following phases:

- *Approach phase*, in which the spacecraft gets in close proximity of the asteroid, and spins up to match the asteroid rate. The objective of this phase is to characterize the asteroid properties and to set up for the close proximity operations.
- *Grapple phase*, in which the capture bag is cinched down, and the motion of the spacecraft catches up with the motion of the asteroid. The asteroid's tumbling motion may be damped by passive energy bleeding.
- *Despin phase*, in which the bag is further tightened around the asteroid, and the asteroid is detumbled and despun using active thrusting. In this phase the system mass properties are managed and the despun state is achieved.
- *Departure phase*, in which the entire asteroid/spacecraft system is placed into a trajectory for transportation to lunar orbit.

GN&C Sequence

The GN&C sequence to achieve these goals includes:

- *Far-field rendezvous and loose station-keeping phase*. This phase is Ground-directed to get safely within a few kilometers, maintain station to within approximately 100 m, and initiate relative position estimation.
- *Spin state and shape characterization phase*. In this phase, closed-loop proximity motions (e.g., circumnavigation) are required. Asteroid characterization is not required to be real-time and can be conducted on the ground.
- *Pre-capture positioning phase*. This phase includes the final approach along an inertially-fixed direction, and translation to the final stand-off point (approximately 50 m) on the approach vector.
- *Synchronize spin phase*, in which the spacecraft is spun up to an appropriate rate to best match the motion of the asteroid.
- *Final translation phase*, closing at constant rate (approximately 0.1 m/s) along the approach vector.
- *Capture phase*, which detects entry of the asteroid into the capture mechanism, controlled stop of translational motion, disable control, and initiate capture.
- *Despin phase*, where closed-loop GN&C is engaged to remove any remaining tumbling motion and to despin the combined system.

Table 1 lists some of the functionality that may need to be considered in the design of the GN&C system.

Approach Strategy

Our focus in this paper is on the grapple phase; in particular, we are interested in the dynamics of the combined asteroid-spacecraft system from the time that contact is first made until the start of the despin phase. The capture dynamics is fundamentally affected by the state of the spacecraft relative to the asteroid at the start of the grapple phase, and it is therefore intrinsically linked to the choice of approach strategy.

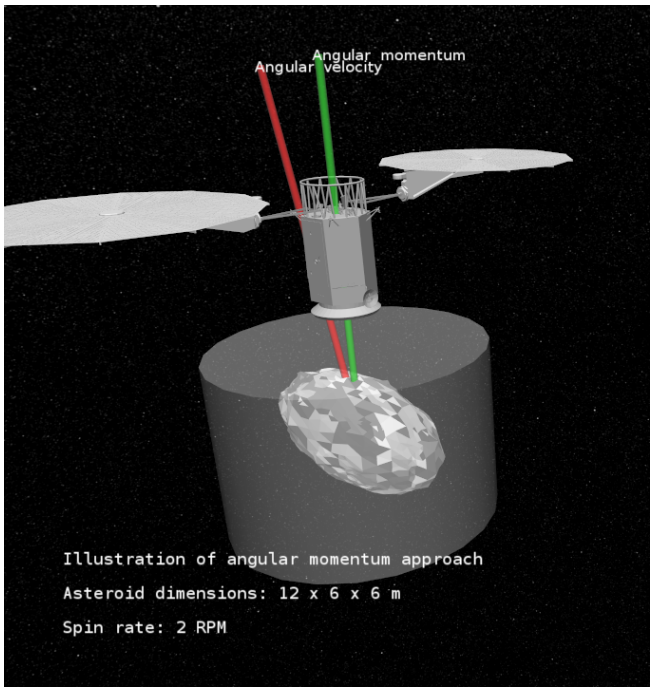

Figure 2. Illustration of the angular momentum approach for a prolate asteroid with an 80° nutation angle. The spacecraft is lined up with the angular momentum vector while matching the precession rate of the asteroid. The time-varying angular velocity traces a cone around the angular momentum vector, but appears constant in the spacecraft frame. The outline of the capture bag (before closing) is shown as a transparent cylinder.

Angular-Momentum Approach—For a simple principal-axis spinner, choosing an approach strategy is straightforward: since the body spins at a constant rate around its angular momentum vector, we may approach along this vector while matching the spin rate, thereby canceling all relative motion between the spacecraft and asteroid.

Asteroid capture GN&C functions

Phase	Sensing	Estimation	Guidance	Actuators	Control	Models
Approach: spacecraft translate	Cameras; laser ranging; closeup illumination; IMU; star tracker	Stereo depth maps; spin-state estimation; attitude filter	Staged approach; best viewing direction; preferred axis	RCS, RWA	3-axis station keep; track approach waypoints; SEP deltaV	Shape; angular momentum; rigid body mass properties
Approach: spacecraft spin-up	IMU; camera; star tracker; LIDAR	Relative state prediction; visual confirmation	Achieve best match to spin	RCS; RWA	3-axis control	Spacecraft mass properties; fuel slosh
Grapple: bag cinch-down	IMU; grapple force/torque sensing	Cinch confirmation	Cinch tension setpoints	Winch line tensioner	Pre-stress to setpoint	Off-line Monte-Carlo analysis of bag/asteroid interaction on multibody system
Grapple: asteroid nutation damping	IMU	Rotational state observer	Track predicted system rotation profile	Winch line tensioner	Tension modulation; winch	Line/bag friction; line viscoelastic damping; fuel slosh
Despin: bag cinch tighten	IMU	Cinch tighten confirm; CM and inertial properties estimation	Cinch tension setpoint; CM adjust; cinch line adjust	Winch line tensioner	Servo tension to setpoint; reposition cinch plane center for system CM adjust	Composite mass properties; fuel slosh; possible thruster articulation
Despin: system detumble/despin	IMU; force/torque sensing at grapple; star tracker	Spin state; spacecraft structure excitation state	Despin profile	RCS; RWA	Minimum-disturbance and minimum-fuel control	Structure flexibility; fuel slosh; thrust allocation
Departure	IMU; star tracker	Spacecraft state; CM and inertia state	Final CM adjust; departure trajectory	Winch line tensioner; SEP; RCS; RWA	Fine position CM; SEP deltaV control	Thrust allocation

Table 1.

One may generalize this approach strategy for a tumbling asteroid by again approaching along the angular momentum vector. In this case, one cannot match the motion of the asteroid precisely, since the angular velocity is not aligned with the angular momentum vector. Instead, one may choose a spin rate that in some sense minimizes the average relative motion. In this project, the angular-momentum approach was considered in the context of inertially axi-symmetrical asteroids, with the spacecraft spin rate chosen according to one of the following strategies:

- *Matching of asteroid precession rate.* By matching the precession rate, the motion of the asteroid relative to the spacecraft is canceled except for the relative spin rate. Thus, the asteroid as seen from the spacecraft appears to stand still, except for a constant spin rate around the symmetry axis of the asteroid. Matching the precession rate may be a good choice for approaching a *prolate* asteroid, since, if it is rotating close to major-axis spin, the relative spin rate will be much smaller than the total spin rate (i.e., the norm of the angular velocity). An illustration of this situation, produced by the Darts/Dshell visualization engine, is shown in Figure 2.
- *Matching of asteroid precession + relative spin rate.* This choice leads to a more complex relative motion between the spacecraft and asteroid, but it may be a good choice for approaching an *oblate* asteroid. If the asteroid is rotating close to major-axis spin, the symmetry axis of the asteroid, as seen from the spacecraft, will trace a cone, while the transverse axes will oscillate with relatively small amplitudes, leading to a "nodding" appearence.

Angular-Velocity Match Approach—Another way to generalize the approach strategy for simple spinners is by matching the angular velocity precisely at a particular epoch. Based on the close observation of the spin state and shape characterization of the target asteroid from the ARV, the future motion of the asteroid is precisely predicted to select an exact future epoch at which to grab it. The approach vector is chosen as the predicted angular velocity vector at this epoch, and the spacecraft spin rate is chosen to match the predicted instantaneous spin rate of the asteroid. The result is that the relative motion between the asteroid and the spacecraft is canceled at the time of capture. A fast-closing capture mechanism is a prerequisite for this strategy, since the relative motion is only canceled for an instant. The freedom in the choice of capture epoch (and thus approach vector and spin rate) can be used, for example, to make the grapple phase more gentle on the spacecraft or to reduce the fuel requirements for the subsequent de-spin. When applying the angular-velocity match approach in this paper, the capture epoch is chosen to minimize the derivative of the angular velocity at the time of capture. Figure 3 illustrates the angular-velocity match approach.

Sideways Grab Approach—Another approach strategy considered in this paper involves approaching along a vector *normal* to the angular momentum vector, without matching any of the rotation of the asteroid. While this strategy may seem counterintuitive, we study it for two primary reasons:

- The sideways grab can be viewed as a worst case of mismatch between the spacecraft and asteroid motion. It is

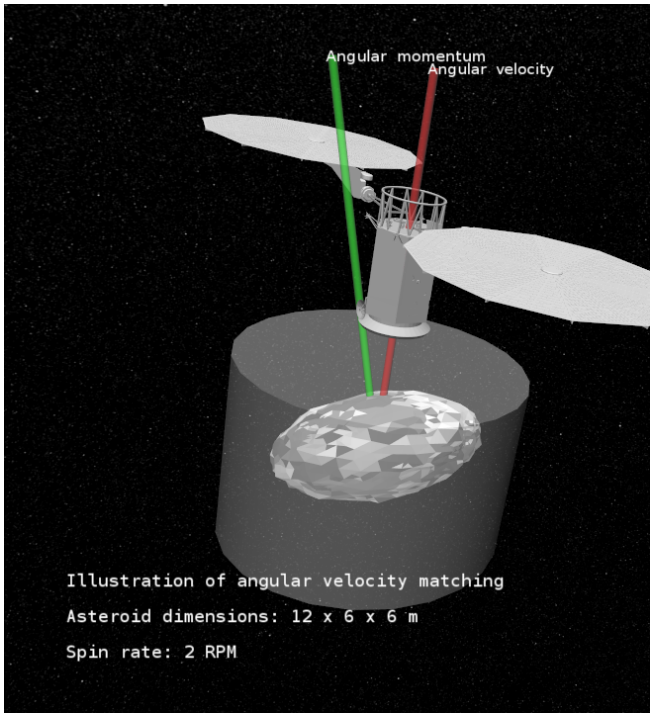

Figure 3. Illustration of the angular velocity match approach for a prolate asteroid with an 80° nutation angle. The spacecraft matches the time-varying angular velocity at a particular epoch.

therefore an interesting bounding case for determining the amount of relative motion that the capture mechanism might be required to tolerate.

• If it can be executed without excessive stress on the spacecraft, the sideways grab strategy is likely to lower fuel requirements for the subsequent despin. Taking a principal-axis spinner as an example, approaching along the angular momentum vector places the spacecraft at the pole of the asteroid with very little leverage for despin. The sideways grab, on the other hand, places the spacecraft at the equator of the asteroid, with maximum leverage for despin.

4. SPIDER-WEB CAPTURE MECHANISM

In this section we discuss a design concept considered early on in the project, which we refer to as the *spider-web* capture mechanism. As described in the introduction, this concept is based around a set of six winch-controlled robotic limbs extending from the spacecraft bus to form a large barrel surrounding the asteroid. Inside the barrel is a drawstring bagging mechanism, similar to a conventional garbage bag, with a number of cinch lines in multiple planes running between the robotic limbs via sleeves on the bag. By tightening the cinch lines using winches on the robotic limbs, the bag closes down on the asteroid, leading to a configuration similar to a cocoon caught in a spider web. The entire capture mechanism is stored in a stowed configuration during launch and while en route to the asteroid, and is deployed prior to capture.

The spider-web design is formed around the idea of using the spacecraft and capture mechanism as a passive damper, to reduce the motion of the combined spacecraft-asteroid system to principal-axis spin without having to fire thrusters. As mentioned in Section 2, the motion of a rotating body with damped flexible modes will tend to converge toward major-axis spin over time, due to energy loss. In the spider-web capture system, sources of energy dissipation are the following:

1. *Viscoelastic damping in the cinch lines*. The cinch lines are designed to be flexible, in order to isolate the spacecraft from the motion of the asteroid and in order to maximize energy dissipation.
2. *Friction between the cinch lines and the capture bag*. The cinch lines are free to slide through the sleeves on the capture bag, opposed only by friction forces contributing toward energy dissipation.
3. *Friction between the bag and the asteroid*. As the bag is closing down on the asteroid, there will be a short period during which the asteroid is scuffing against the inside of the bag.
4. *Hysteretic damping in the robotic limbs*. As the robotic limbs flex due to changing tensions in the cinch lines, hysteretic damping contributes toward energy dissipation.
5. *Other flexible modes*. Examples include fuel slosh and solar panel flexing.

Model Description

Here we describe a simulation model built with the primary goal of gaining a qualitative understanding of the damping properties that might be achieved with the spider-web capture mechanism. Among the sources of energy dissipation mentioned above, we focus only on items 1 and 2, since these are thought to be most significant. Here and in subsequent simulations, it is assumed that the closing of the bag around the asteroid happens instantaneously, so that no scuffing occurs between the asteroid and the bag. This choice is made deliberately, for the following reasons:

• Accurate modeling of the friction between the asteroid and the bag is difficult, if not impossible, to achieve.
• A design driver for the system is to have only engineered surfaces undergo sliding friction, since it is believed that any significant sliding friction with the asteroid increases mission risk and the required analysis.
• When simple friction models are included between the asteroid and the bag, the result is generally a more desirable behavior (due to increased energy dissipation and easing of the impact of the initial grab). The omission of bag-asteroid friction is therefore thought of as a bounding case.

Figure 4 shows an annotated overview of the model produced by the Darts/Dshell visualization engine. The spacecraft bus is represented by a solid cylinder, with six robotic limbs attached. Although each limb is modeled by a sequence of seven cylindrical elements, the connecting joints are frozen for the simulations presented here, thereby turning the spacecraft bus and the limbs into a single rigid body. The asteroid is also modeled by a solid cylinder, meaning that for this case we are considering only inertially axi-symmetrical asteroids.

The interaction between the spacecraft and the asteroid is modeled by a set of of 18 cinch lines, each of which is attached to two robotic limbs (spaced 120° apart) and runs via a *virtual hoop* attached to the asteroid. The virtual hoop acts like a physical hoop, in that it allows the cinch line to slide freely in one degree of freedom, opposed only by Coulumb-type friction forces, while the motion is restricted in the other two degrees of freedom. Cinch line tension is modeled by a spring-damper, with restoring forces proportional to the total length of the cinch line (minus the nominal, or unsprung,

length), and viscoelastic damping forces proportional to the derivative of this length. Figure 5, which shows the asteroid and capture mechanism as seen from the spacecraft point of view, gives a better picture of how a single cinch line attaches to the limbs and to the asteroid.

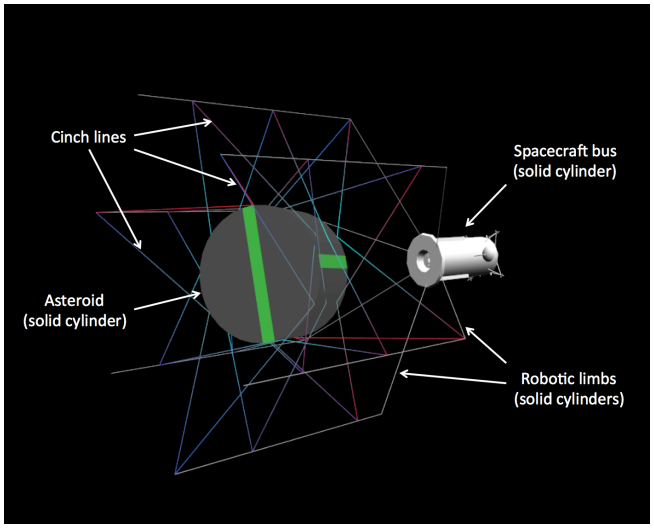

Figure 4. An overview of the Darts/Dshell simulation model for the spider-web capture mechanism, illustrating the spacecraft, asteroid, robotic limbs, and the cinch line-hoop interaction model

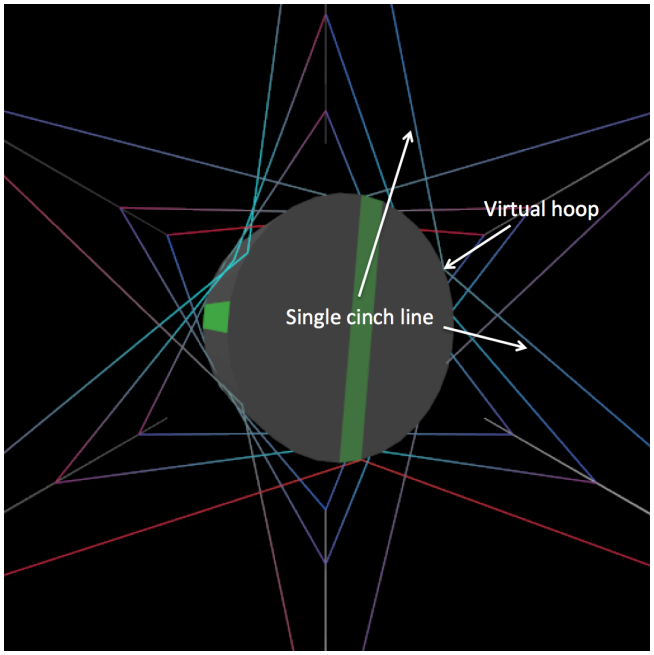

Figure 5. The asteroid and capture system as seen from the spacecraft point of view

The approach strategy considered at this stage is the angular-momentum approach.

Results

The adjustable parameters for the capture mechanism are the stiffness and damping constants, as well as the nominal length (or, equivalently, the pre-stress), of the cinch lines, together with the friction coefficient (the ratio of friction force to normal force) for the cinch line-hoop interaction. A number of point simulations were conducted with selected parameterizations for the capture mechanism, combined with different asteroid inertial properties and initial states. The main conclusions from these simulations are the following:

Simulation parameters, spider-web example

	Value	Unit
Asteroid		
Mass	500,000	kg
Radius	3.5	m
Height	3	m
Spin rate	1	deg/s
Nutation angle	30	deg
Spacecraft		
Mass	15,000	kg
Bus height	6	m
Bus radius	1.5	m
Distance of CM to asteroid CM	13.5	m
Capture mechanism		
Cinch line stiffness constant	2	N/m
Cinch line damping constant	15	N/(m/s)
Cinch line pre-stress	2	N
Cinch line-hoop friction coefficient	0.1	1

Table 2.

- For the limited number of cases studied, the simulations confirmed that the tumbling motion of the asteroid was asymptotically damped out, so that the overall system converged toward major-axis spin.
- In order to achieve damping on a time scale of a few days, the cinch lines were chosen to be very flexible, thus allowing for a large amount of relative motion. It is not clear whether the resulting system would be physically realizable with space-qualified materials.
- In the simulation model used, the energy dissipation is dominated by viscoelastic damping; changes in the friction coefficient have a more limited effect on the outcome.
- The combined spacecraft-asteroid system tends to converge toward a flat spin, where the axis of rotation is close to normal to the symmetry axis of the spacecraft bus. This is considered desirable, since it increases the thruster lever arm for subsequent de-spin.[2]

As an example to illustrate these points, we present simulation results for a specific case defined by the parameters listed in Table 2. In this example, the angular momentum vector points directly along the inertial z axis. Figure 6 shows the angular velocity of the asteroid, in inertial coordinates, over a 48-h period after the capture. It can be seen that the angular velocity starts with both a z component and a smaller component in the x-y plane. Over time, the x and y components are damped due to energy loss, and the angular velocity will eventually converge toward simple spin around the inertial z axis. Figure 7 similarly shows the angular velocity of the spacecraft. Because the spacecraft has

[2]Note that this is a function of the mass geometry of the combined spacecraft-asteroid system—by adding the mass of the spacecraft to the asteroid, the major axis of the combined system may be shifted.

approached the asteroid along the angular momentum vector, it starts out with simple z axis spin. It gains an x and y component through the interaction with the asteroid, before slowly converging toward simple z-axis spin as the tumbling motion dies out.

Figure 8 shows the total energy of the system, including the kinetic energy of the asteroid and spacecraft and the potential energy of the cinch lines. As expected, the energy is strictly decreasing. Finally, Figure 9 shows the angle between the asteroid symmetry axis and the angular momentum axis, and the angle between the spacecraft symmetry axis and the angular momentum axis. From this plot it can be seen that the system is settling close to a flat spin.

From Figures 6–9 it looks as though the motion stabilizes after only a few hours. Indeed, most of the initial relative motion has been damped out at this point, but the system is spinning in an unstable pattern close to a minor axis of the combined system. This instability eventually leads to further excitation of the capture mechanism and convergence toward major-axis spin.

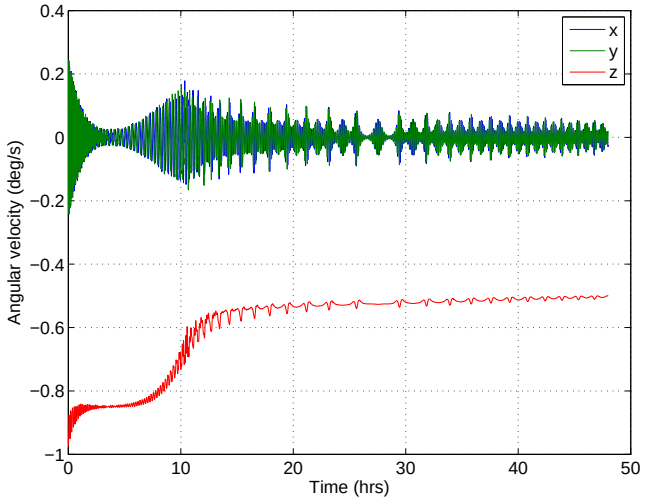

Figure 6. Angular velocity of asteroid in inertial coordinates

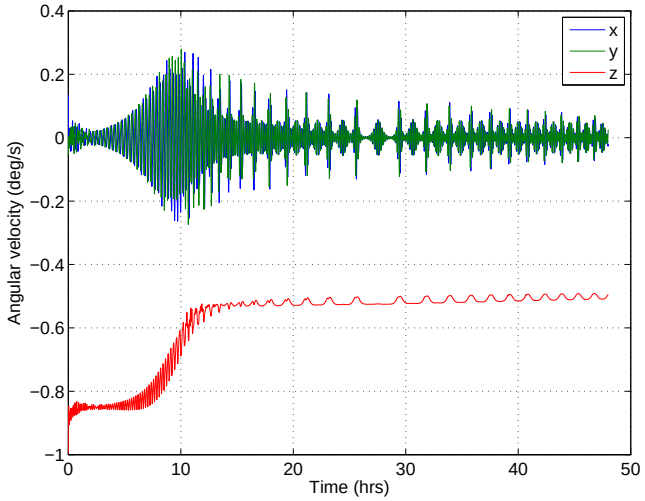

Figure 7. Angular velocity of spacecraft in inertial coordinates

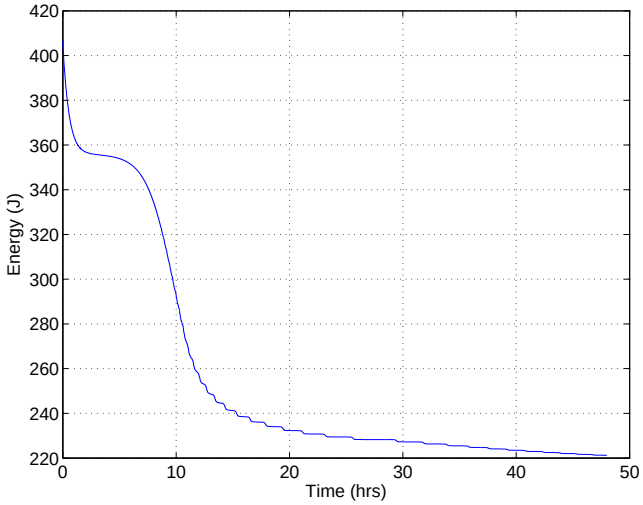

Figure 8. Total kinetic and potential energy

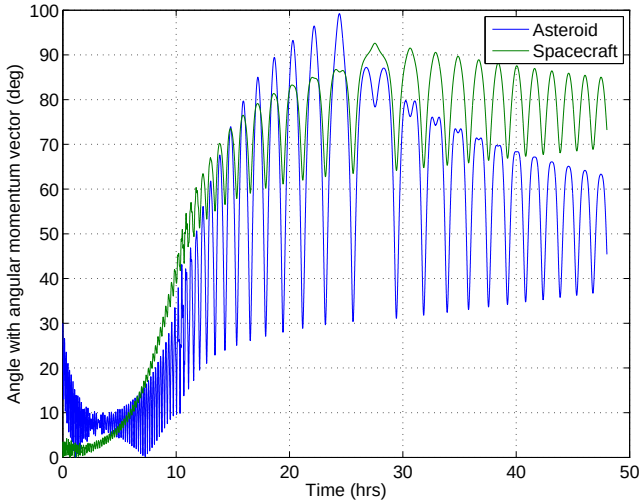

Figure 9. Angle between symmetry axis and angular momentum vector for asteroid and spacecraft

5. Inflatable Capture Mechanism

The spider-web capture design was set aside early in the project due to mechanical design and packaging considerations, related in part to the complexity introduced by the large number of robotic limbs and cinch lines. In this section, we consider a different design, in which the robotic limbs have been replaced by an inflatable exoskeleton with a built-in capture bag.

The inflatable mechanism is to be deployed shortly before initiating the asteroid capture, and takes a form similar to the robotic limbs, consisting of a conical section and a barrel section. The bag and the inflatable members supporting it are designed to rapidly collapse around the asteroid with the help of circumferential and axial winch cords sown into the fabric. Once the bag is closed up, the spacecraft and asteroid are kept apart by collapsed fabric and inflatable members that act as an isolation device between the asteroid and the spacecraft.

Model Description

The inflatable capture mechanism is modeled by attaching two sets of linear spring-dampers directly between the spacecraft bus and the asteroid, as illustrated in Figure 10. There are six attachment points around the lower perimeter of the spacecraft bus, and six corresponding attachment points on the asteroid, located on a circle around the asteroid center of mass (CM) in a plane normal to the vector between the asteroid and spacecraft CMs. Twelve spring-dampers are criss-crossed between the attachment points on the spacecraft and the attachment points on the asteroid. Another six spring-dampers are attached directly between the attachment points on the spacecraft and the corresponding attachment points on the asteroid. The two sets of spring-dampers are illustrated by the red and blue lines in Figure 11.

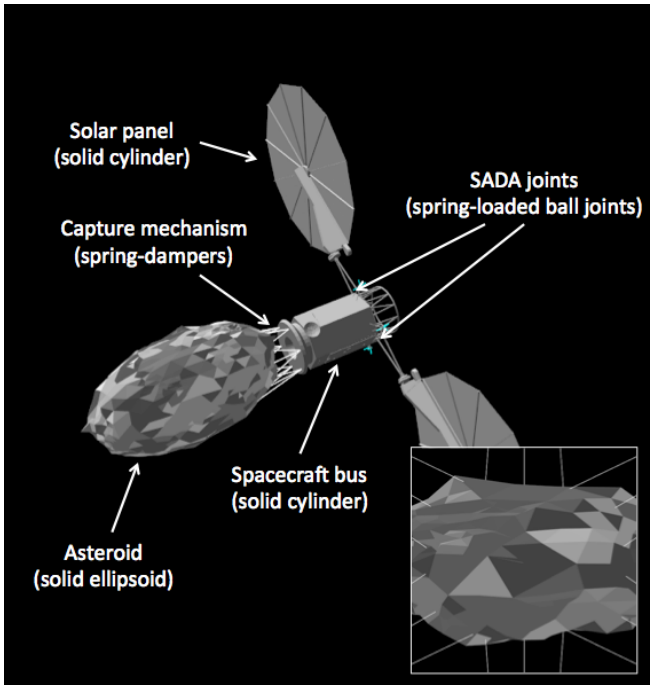

Figure 10. An overview of the Darts/Dshell simulation model for the inflatable capture mechanism, illustrating the spacecraft, asteroid, solar panels, and the spring-dampers. The inset shows the asteroid and capture mechanism as seen from the spacecraft point of view.

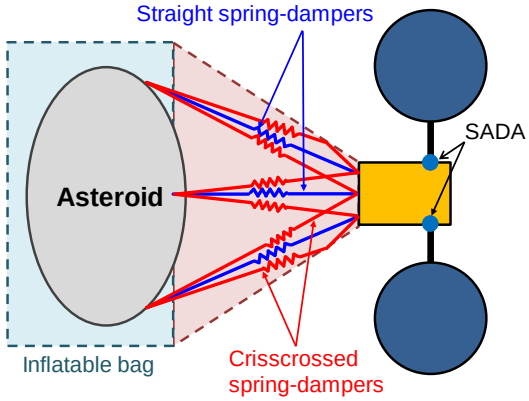

Figure 11. Inflatable capture mechanism model

Simulation parameters, inflatable example

	Value(s)	Unit
Asteroid		
Mass	1,000,000	kg
Semi-axes	6, 6, and 3	m
Spin rate	2	RPM
Nutation angle	0	deg
Spacecraft		
Mass	15,000	kg
Bus height	6	m
Bus radius	1.5	m
Distance of CM to asteroid CM	10	m
Capture mechanism		
Stiffness, criss-crossed lines	4,000	N/m
Damping, criss-crossed lines	700	N/(m/s)
Stiffness, straight lines	5,000	N/m
Damping, straight lines	900	N/(m/s)
Asteroid attachment radius	3.5	m

Table 3.

The spring-damper configuration was originally motivated by a particular design, in which the criss-crossed lines represented a combination of axial winch cords and collapsed bag fabric, and the straight lines represented inflatable struts. However, as the design evolved, the spring-dampers came to represent an inflatable isolation device between the spacecraft and the asteroid in a more abstract sense.

Also shown in Figure 10 are solar panels that have been added to the model. The solar panels are modeled as thin cylinders mounted on zero-mass booms, which are attached to the spacecraft bus via 3-DOF ball joints. The ball joints are endowed with 3-DOF torsional spring-dampers with stiffness and damping constants set according to parameters received by the manufacturer.

The asteroid is modeled as a solid ellipsoid with three separately adjustable semi-axes, allowing us to represent any tri-inertial rigid object. As before, it is assumed that the capture itself takes place instantaneously, by attaching the spring-dampers between the spacecraft and the asteroid at a particular epoch.

A set of example parameters, which we shall refer to throughout the rest of this section, is given in Table 3.

Relationship to Physical System

Given that the simulation model is an abstraction of the true physical system, it is pertinent to ask how a quantitative relationship between the two can be established. One way of doing so is by deriving system-level stiffness and damping parameters of the model in different degrees of freedom, and comparing these to corresponding values for the physical system, derived from more complex soft-goods modeling or experiments. The results of this comparison can be used to adjust the simulation model to match the properties of a particular design, and, conversely, to synthesize design requirements that must be met by the mechanical system.

To obtain system-level stiffness and damping constants for the capture mechanism, we consider the changes in restoring

forces and damping forces due to small deflections of the spacecraft's position and attitude relative to the asteroid, around a setpoint defined by the nominal spring-damper lengths and zero velocities. Letting f_r and τ_r denote the 3-dimensional vectors of restoring forces and torques with respect to some reference point, and letting Δp and $\Delta\Theta$ denote the three-dimensional vectors of relative position and attitude deflections with respect to the same reference point, it can be shown that the Jacobian of $[f_r;\tau_r]$ with respect to $[\Delta p;\Delta\Theta]$ is given by

$$-\begin{bmatrix} \sum_{i=1}^{N} k_i e_i e_i^{\mathsf{T}} & \sum_{i=1}^{N} k_i e_i e_i^{\mathsf{T}} S(r_i)^{\mathsf{T}} \\ \sum_{i=1}^{N} k_i S(r_i) e_i e_i^{\mathsf{T}} & \sum_{i=1}^{N} k_i S(r_i) e_i e_i^{\mathsf{T}} S(r_i)^{\mathsf{T}} \end{bmatrix},$$

where N is the number of spring-dampers, k_i is the stiffness constant of spring-damper i, e_i is the unit vector pointing from the attachment point of spring-damper i on the spacecraft to the attachment point on the asteroid, and r_i is the vector from the reference point to the attachment point of spring-damper i on the spacecraft. The function $S(\cdot)$, which maps from $\mathbb{R}^3$ to the set of 3×3 skew-symmetric matrices, is such that $S(x)y = x\times y$ for all $x,y\in\mathbb{R}^3$. We refer to the negative of the Jacobian as the stiffness matrix K. Similarly, letting f_d and τ_d denote damping forces and torques, the Jacobian of $[f_d;\tau_d]$ with respect to the vector $[\Delta v;\Delta\omega]$ of velocity and angular velocity deflections is given by

$$-\begin{bmatrix} \sum_{i=1}^{N} c_i e_i e_i^{\mathsf{T}} & \sum_{i=1}^{N} c_i e_i e_i^{\mathsf{T}} S(r_i)^{\mathsf{T}} \\ \sum_{i=1}^{N} c_i S(r_i) e_i e_i^{\mathsf{T}} & \sum_{i=1}^{N} c_i S(r_i) e_i e_i^{\mathsf{T}} S(r_i)^{\mathsf{T}} \end{bmatrix},$$

where c_i is the damping constant of spring-damper i. We refer to the negative of this Jacobian as the damping matrix C.

If we consider a nominal parameterization described in Table 3, using the spacecraft CM as the reference point, we obtain the following stiffness and damping matrices:

$$K \approx \begin{bmatrix} 4943 & 0 & 0 & 0 & 8103 & 0 \\ 0 & 4943 & 0 & -8103 & 0 & 0 \\ 0 & 0 & 68113 & 0 & 0 & 0 \\ 0 & -8103 & 0 & 79928 & 0 & 0 \\ 8103 & 0 & 0 & 0 & 79928 & 0 \\ 0 & 0 & 0 & 0 & 0 & 17034 \end{bmatrix},$$

$$C \approx \begin{bmatrix} 871 & 0 & 0 & 0 & -1406 & 0 \\ 0 & 871 & 0 & 1406 & 0 & 0 \\ 0 & 0 & 12059 & 0 & 0 & 0 \\ 0 & 1406 & 0 & 14015 & 0 & 0 \\ -1406 & 0 & 0 & 0 & 1415 & 0 \\ 0 & 0 & 0 & 0 & 0 & 2981 \end{bmatrix}.$$

Considering, for example, the translational mode along the z axis, we see that this mode is decoupled from the other modes, and has a system-level stiffness of $68,113$ N/m; this number is within the limits of what can be achieved using an inflatable isolation device. We also see that the system-level damping in this mode is $12,059$ N/(m/s), which translates into a relative system-level damping of $\zeta \approx 19\%$ for a $1,000,000$ kg asteroid. This is a fairly high level of damping, though it may still be achievable with an inflatable isolation device.

Results

The simulation model has been exercised with a large number of asteroid and capture mechanism parameterizations. Some initial conclusions from these simulations were the following:

- Compared to the spider-web capture system, much stiffer spring-dampers are required in order to keep the asteroid and spacecraft separated. This is due to the difference in capture geometry—the spacecraft "pinches" the asteroid through a narrow set of directions, using lines connected directly to the spacecraft bus, instead of grabbing it from multiple directions with the help of the rigid robotic limbs.
- The spring-dampers must be arranged in a geometry that yields torsional stiffness around the z axis of the spacecraft, hence the criss-crossing of the lines in the first set of spring-dampers.
- The need for stiffer spring-dampers effectively rules out relying on viscoelastic damping for detumbling the asteroid. Thus, our investigation naturally focused on a "quick-grab" strategy of rapidly catching up to the motion of the asteroid in preparation for active detumble/despin using the spacecraft thrusters.
- Capturing the asteroid using a stiff capture mechanism results in a greater impact on the spacecraft immediately after grabbing the asteroid. A primary consideration is therefore the torque applied at the ball joints connecting the solar array booms to the spacecraft bus. These are compared to the SADA torque tolerances, for which an upper limit of $1,765$ Nm in each axis is assumed.

The dynamics of the system after the grab takes place can be divided into two phases: a transient phase, in which the capture mechanism undergoes large deflections to absorb the relative motion between the spacecraft and asteroid; and a semi-steady-state phase, in which the asteroid and spacecraft act almost as a single rigid body, with very small deflections of the capture mechanism. Analysis and simulation of the semi-steady-state phase show that the SADA joint torques remain below the upper limit of $1,765$ Nm even for worst-case asteroids, but the transient phase is more challenging.

When investigating the dynamics of the transient phase, we focused to a large extent on the sideways grab. There are two reasons for this, as mentioned in Section 3: (i) it represents the worst case of mismatch between the motion of the asteroid and the spacecraft, and it is therefore a good bounding case; and (ii) this type of approach is of interest because of the improved lever arm (and consequently reduced fuel requirements) during the subsequent de-spin.

Figure 12 shows the SADA joint torques for one of the solar panels for the sideways grab, using the parameterizations listed in Figure 3. In this example, the asteroid is spinning at 2 RPM, the presumed upper bound on the spin rate. It can be seen that the maximum torque far exceeds the limit of $1,765$ Nm.

We are interested in seeing how the maximum torque changes when adjusting the stiffness of the capture mechanism. Figure 13 shows the maximum torque for the same example as in Figure 12, but with the stiffnesses of both sets of spring-dampers multiplied by factors between 0.1585 and 10 while keeping the damping ratios constant. Neither stiffening nor softening the mechanism is sufficient for reducing the torques to acceptable levels (softening the springs further leads to collision between the spacecraft and asteroid).

In general, the simulations indicate that, using the sideways grab strategy, the torques can be kept within acceptable limits for simple spinners up to approximately 1 RPM. When the asteroid is tumbling, the limits are exceeded for lower spin rates. Thus, the sideways grab is unlikely to be a viable practical strategy for fast spinners.

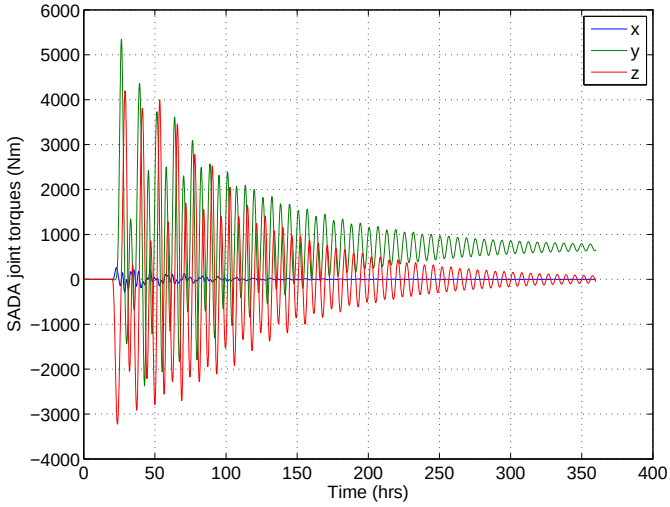

Figure 12. SADA joint torques for panel 1 during sideways grab at 2 RPM. The maximum torque far exceeds the limit of 1,765 Nm.

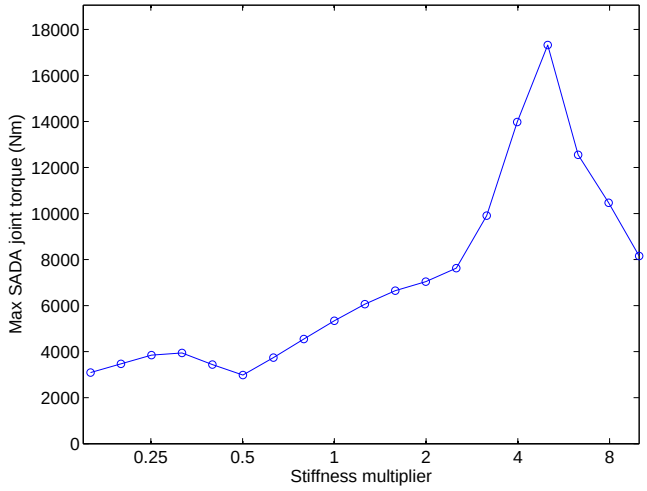

Figure 13. Max SADA joint torques for panel 1 for a range of stiffness multipliers

6. Abstract 6-DOF Joint

We next describe the abstract 6-DOF joint model. Here we assume that the capture bag is rigidly attached to the asteroid and connected to the ARV by an isolation device. Instead of assuming a specific design of the isolation device, we model it by an abstract 6-DOF joint consisting of three translational and three rotational linear spring-dampers, as illustrated in Figure 14. A design of the 6-DOF joint is fully specified by twelve parameters: the spring and damping coefficients for each of the six degrees of freedom. We denote the translational and rotational spring coefficients by K_x^T, K_y^T, K_z^T, K_x^R, K_y^R, and K_z^R. Likewise, we denote the translational and rotational damping coefficients by C_x^T, C_y^T, C_z^T, C_x^R, C_y^R, and C_z^R. As we explain shortly, we impose constraints on these coefficients in order to keep them within bounds that are physically realistic for an inflatable isolation device.

The objective of this abstract modeling approach is to better exploit the design space of the isolation device. A drawback

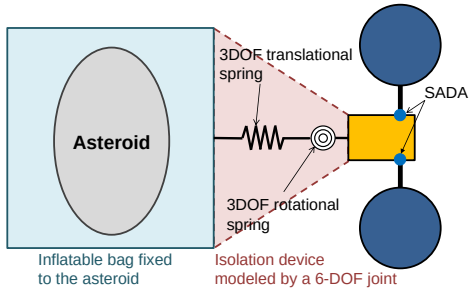

Figure 14. The 6-DOF joint model of the flexible isolation device.

of the approach outlined in the previous section is that the relationship between the stiffness and damping in different degrees of freedom is dictated by the geometrical configuration of the spring-dampers. With the 6-DOF joint, the stiffness and damping in the three translational and three rotational degrees of freedom can be specified directly and independently. As we describe in detail in the next section, the design parameters of the 6-DOF joint are tuned systematically through optimization.

We ensure that the stiffness in each degree of freedom is physically realizable by enforcing upper and lower bounds as well as symmetry constraints. Specifically, the rotational spring constants are bounded between 100,000 Nm/rad and 5,700,000 Nm/rad, while the translational spring constants are bounded between 5,000 N/m and 80,000 Nm. Since the isolation device must be symmetric about the ARV's z axis, we enforce the following symmetry constraints: $K_x^T = K_y^T$ and $K_x^R = K_y^R$. We also limit the damping coefficients to keep system-level damping percentages in the single digits. For later convenience, we denote the spring coefficients in the x and y axes as K_{xy}^T and K_{xy}^R.

As in the previous section, we initially investigated the sideways grab approach, but it turned out that the requirements are not satisfied by any parameter values within the bounds described above. Instead, in the rest of this paper we focus on the angular-velocity match approach, which was described in Section 3.

7. Design Optimization

In this section we explain how we tune the design parameters of the 6-DOF joint model of the isolation device so that all the given requirements are satisfied. Our approach is to pose the design problem as a constrained optimization problem and solve it by using a genetic algorithm. Although we focus on the 6-DOF joint model in this paper, the optimization-based approach is not specific to a particular model, hence it can be used for broader classes of design problems.

Requirements

Table 4 summarizes the requirements imposed on our design problem. The first two requirements come from vehicle safety while the rest are required to keep the stiffness within physically reasonable bounds.

The maximum allowable SADA torques are 1,765 Nm in each axis, as mentioned in the previous section. The *deflection*

Optimization requirements

	Symbol	Lower bound	Upper bound	Unit
SADA joint torques	$T^{\text{SADA}}_{x,y,z}$	-	1,765	Nm
Deflection angle	θ	-	45	deg
Lateral stroke	l^L	-	1.0	m
Axial stroke	l^A	-	2.0	m
Translational spring coefficients	$K^T_{xy,z}$	5,000	80,000	N/m
Rotational spring coefficients	K^R_{xy}	100,000	570,000	Nm/rad
	K^R_z	100,000	5,700,000	Nm/rad

Table 4.

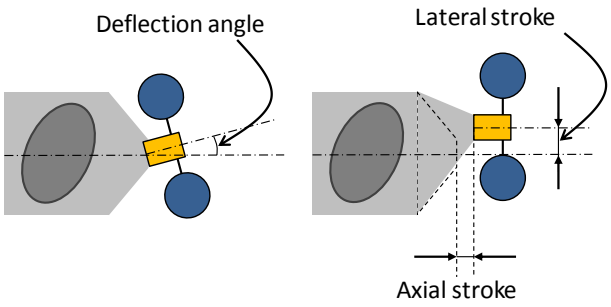

(a) Deflection angle (b) Lateral and axial strokes

Figure 15. Definitions of optimization metrics

angle of the ARV, which is illustrated in Figure 15(a), is defined as the angle of rotation between the spacecraft and asteroid, with zero rotation defined by the relative attitude at the start of the capture. The deflection angle must be limited to 45° in order to ensure adequate clearance with the asteroid. The *lateral and axial strokes* are the deflections of the translational spring in the 6-DOF joint model in lateral (i.e., x and y) and axial (i.e., z) directions, respectively, as shown in Figure 15(b). We constrain the lateral stroke to 1 m and the axial stroke to 2 m. We denote the SADA torque, the deflection angle, the lateral stroke, and the axial stroke at time t by $T^{\text{SADA}}_i(t)$, $\theta(t)$, $l^T(t)$, and $l^A(t)$, respectively, where $i = x, y, z$. As we discussed in the previous section, we impose upper and lower bounds on the structural spring coefficients for the sake of physical realizability, as shown in the table.

Throughout the rest of the paper we denote by $\overline{\cdot}$ and $\underline{\cdot}$ the upper and lower bounds of a variable.

We consider asteroids with initial spin rates of up to 2 RPM and mass of up to $1,000,000$ kg. Within this range, the requirements specified above must be robustly satisfied for all possible moments of inertia and spin states.

Optimization Problem Formulation

Given the requirements specified above, we next formulate a constrained optimization problem that is solved to obtain a feasible set of design parameters. In particular, we pose the optimization problem as a minimization of the deflection angle with constraints on SADA torques, lateral and axial strokes, and spring coefficients, as follows:

$$\min_t \max \theta(t)$$

over

$$\underline{K_i^T} \le K_i^T \le \overline{K_i^T}, \quad \underline{K_i^R} \le K_i^R \le \overline{K_i^R}, \quad i = xy, z$$

subject to

$$\max_t T_i^{\text{SADA}}(t) \le \overline{T_i^{\text{SADA}}}, \quad i = x, y, z$$

$$\max_t l^T(t) \le \overline{l^T}, \quad \max_t l^A(t) \le \overline{l^A}$$

Note that θ, T^{SADA}, l^T, and l^A are time-varying variables. Therefore, their maximum over time must be below the specified upper bound. Also note that we minimize the maximum deflection angle, $\max_t \theta(t)$, instead of imposing a hard constraint on it. After solving the optimization problem, we check if the resulting maximum deflection angle is below the specified upper bound. If not, the design problem is infeasible.

The optimization problem can be formulated in other ways, for example, a minimization of one of the SADA joint torques while imposing constraints on the other SADA torques and the deflection angle. In general, the objective function should reflect the preference among feasible solutions. We chose the deflection angle as the objective function because it is considered to be preferable to have smaller deflection angle in order to minimize the risk of total loss of the ARV due to a collision with the asteroid. It is also possible to employ a more complicated preference metric consisting of multiple variables.

Evaluation of Objective and Constraint Functions using Darts/Dshell

We use Darts/Dshell in order to evaluate $\theta(t)$, $T_i^{\text{SADA}}(t)$, $l^A(t)$, and $l^T(t)$ in the optimization problem formulated above. We create physics models of the ARV and an asteroid, whose physical properties are specified by adjustable parameters.

As described in the previous section, we need to evaluate the maximum of the objective and constraint functions over time. Therefore, we must fully simulate the transient response, which starts at the time of contact between the capture device of the ARV and the asteroid and typically lasts for ~ 100 s. This simulation must be performed at each iteration of the optimization. Its typical running time is 5–10 s.

Optimization Method

Building upon Darts/Dshell, we have recently developed the Darts/Dshell Optimizer that is capable of solving the optimization problem formulated above. Figure 16 shows the block diagram of our iterative optimization system. An optimization algorithm specifies a set of design parameters, which in our case include spring coefficients. Then the Darts/Dshell simulator is called as a subroutine that takes the design parameters as inputs and outputs the objective and constraint function values (i.e., $\theta(t)$, $T_i^{\text{SADA}}(t)$, $l^A(t)$, and $l^T(t)$). The optimization algorithm takes them as inputs, and use the inputs to adjust the design parameters in order to refine the solution. This iteration is repeated until convergence to an optimal solution. It can handle both constrained and unconstrained optimizations.

We employ a genetic algorithm (GA) [5] to implement the Darts/Dshell Optimizer. A third-party implementation called

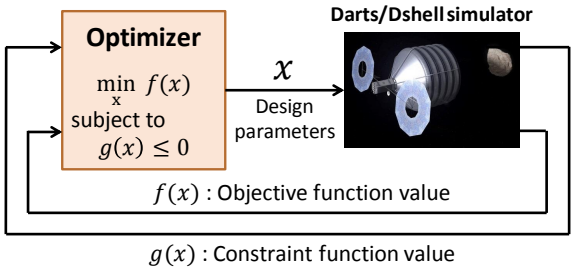

Figure 16. The architecture of the Darts/Dshell Optimizer. It is an iterative process in which a Darts/Dshell simulator is called by the optimizer as a subroutine to evaluate objective and constraint functions.

the Matlab Genetic Algorithm Toolbox developed by [6] is used. GA is a metaheuristic optimization algorithm that mimics the process of natural selection. At each iteration (called a *generation* in a GA context), it populates individuals (i.e., candidate solutions) that have different *genes*, which are essentially the decision variables (design parameters in our case). The objective and constraint function values of every individual are evaluated, and high-performing individuals generate offspring to form the next generation. Genetic algorithms have been successfully applied for design problems in various domains, including spacecraft design [7], [8], [9].

In our case, the Darts/Dshell simulator is run to evaluate the objective and constraint function values for *each* individual at *every* generation. As a result, it typically takes a few hours to solve the optimization problem formulated above. In order to reduce the computation time, we implement a parallel computation capability on the Darts/Dshell Optimizer.

Robust Optimization

As mentioned earlier, the requirements must be robustly satisfied for all possible mass properties (i.e., moments of inertia) and spin states. However, although performing a robust optimization with GA is possible, it requires order-of-magnitude longer computation time than a regular GA. Instead, we obtain a robustly feasible solution as follows. First we heuristically find a "hard problem," meaning a combination of a mass property and a spin state that tends to result in a large deflection angle, SADA torques, and lateral and axial strokes. Of course, the satisfaction of the constraints at this "hard problem" does not guarantee the satisfaction of the constraints at the worst case. In order to address this issue, we solve the "hard problem" with tightened constraints. The difference between the original constraint boundaries and the tightened boundaries works as a safety margin. Finally, we check the robust feasibility of the solution by conducting a parametric sweep over all possible combinations of the mass property and spin rate, discretized at appropriate intervals. The result of the parametric sweep is described in detail in Section 8.

The "hard problem" that we found is with an oblate ellipsoid whose major and minor semi-axis lengths are 6.5 m and 1.95 m, respectively, as shown in Figure 17. The major axis of the asteroid is rotated by 60° from the angular momentum vector. The spin rate is 2 RPM and the mass is 10^6 kg. This configuration is "hard" because it represents a severely a tumbling rotation. We tightened the upper bound on the SADA torques to 1,700 Nm.

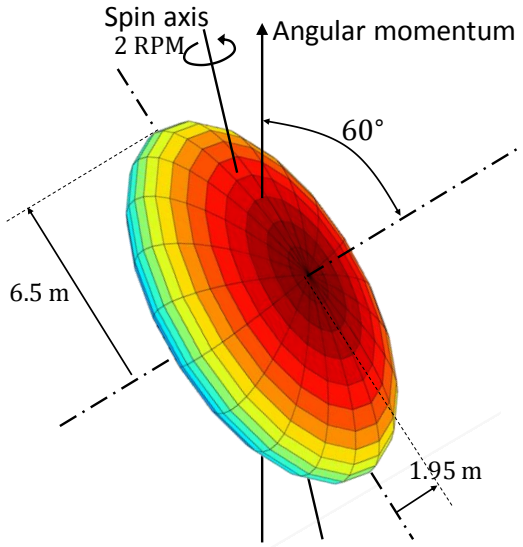

Figure 17. The oblate asteroid model and its initial attitude against which the design variables are optimized. Since this configuration results in severe tumbling motion, it is considered to be one of the most challenging cases within the family of asteroids under consideration.

Optimized parameters

	Symbol	Value	Unit
Translational spring coefficients	K_{xy}^T	7,900	N/m
	K_z^T	7,300	N/m
Rotational spring coefficients	K_{xy}^R	570,000	Nm/rad
	K_z^R	4,630,000	Nm/rad

Table 5.

Optimization Result

By solving the optimization problem formulated above with the Darts/Dshell Optimizer, we obtained the solution shown in Table 5.

Note that the resulting design has low translational stiffness but high rotational stiffness. This result is qualitatively explained as follows. The low translational stiffness helps to reduce the SADA torque by slowing the transient response, but increases lateral and axial strokes. The Darts/Dshell Optimizer chose the smallest translational spring coefficients that do not violate the constraints on strokes. On the other hand, large rotational spring constants were chosen in order to minimize the deflection angle.

Figure 18 shows the time series data of the SADA joint torques, the deflection angle, and the lateral and axial stroke with the optimized design variables and the asteroid's initial configuration shown in Figure 17. The horizontal axis of the figure is the elapsed time since the contact between the asteroid and the ARV. As can be seen from the plots, all the requirements are satisfied over this period. Note that the SADA torque about the y axis and the lateral stroke is very close to the constraint boundary, while the deflection angle is well below its upper bound. This result is expected because we formulate the optimization problem as a minimization of

deflection angle with hard constraints on the SADA torques and the strokes. Irregular transient responses are observed for approximately 50 s after the contact. Then follows an oscillatory behavior with approximately 80-s period.

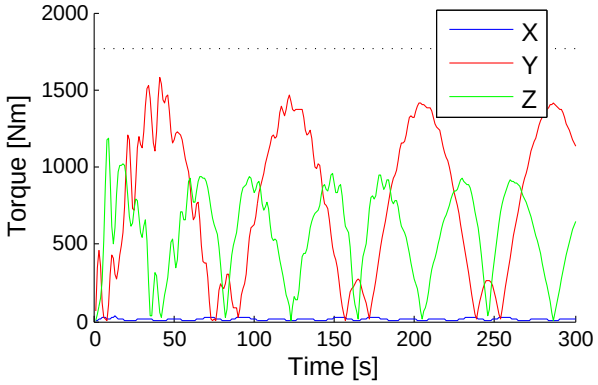

(a) SADA joint torques (absolute values)

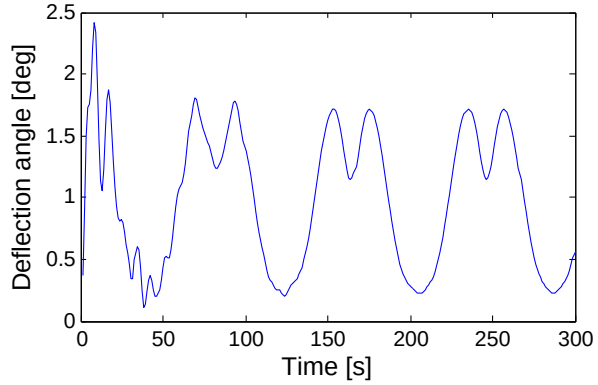

(b) Deflection angle

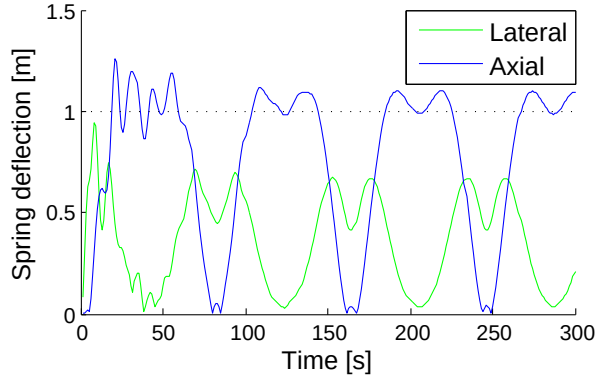

(c) Lateral and axial strokes (absolute values)

Figure 18. The time-series plots of the SADA torques, deflection angle, and spring deflections

8. PARAMETRIC SWEEPS

In this section we perform a parametric sweep over the mass properties and the spin state of the asteroid in order to verify that the solution obtained in the previous section robustly satisfies the given requirements.

By mass property we mean the mass and the moments of inertia of the asteroid. We assume that the mass is at the upper bound, $1,000,000$ kg. Without loss of generality we assume that the principal axes correspond to the x, y, and z axes of the asteroid's body frame. The ARV's dynamic behavior is influenced by the asteroid's mass, moments of inertia, and spin state, but not its shape. Therefore we assume without loss of generality that the asteroid is a solid ellipsoid. Its moments of inertia is fully specified by the length of its three semi-axes, which are denoted by r_x, r_y, and r_z. We assume $r_x \geq r_y \geq r_z$ and fix r_x to its upper bound, 6.5 m. We let $r_y = k_y r_x$ and $r_z = k_z r_x$, and we vary k_y and k_z within a range $0.3 \leq k_y \leq k_z \leq 1$ with an interval of 0.1.

As for the spin state, we assume that the angular velocity is aligned with the z axis of the inertial frame. We specify the initial attitude of the asteroid by Euler angles relative to the inertial frame, denoted by α (about the x axis), β (y axis), and γ (z axis). We sweep over 38 initial attitudes, 19 of which are with $\beta = \gamma = 0$ and $\alpha = 0, 5^\circ, 10^\circ, \ldots, 90^\circ$ while the others are with $\alpha = \gamma = 0$ and $\beta = 0, 5^\circ, 10^\circ, \ldots, 90^\circ$. The spin rate is varied from 0.5 RPM to 2 RPM with an interval of 0.5 RPM. This results in $5,472$ combinations in total.

Figure 19 shows the result of the parametric sweep. In all the $5,472$ cases, the requirements are fully satisfied.

9. CONCLUDING REMARKS

The results of Section 8 suggest that, with a properly designed capture mechanism, it is indeed possible to handle the range of asteroids baselined for this study without giving rise to excessive loads on critical spacecraft components. Figure 19 does indicate that the SADA torque margins are relatively small; however, as explained in Section 7, the capture mechanism parameters were not chosen to minimize the torques, but to minimize the deflection angle subject to the torque constraint. Moreover, some of the worst-case scenarios may be considered unlikely enough to be excluded from future consideration. The asteroids resulting in the highest SADA torques tend to have the following characteristics:

- High spin rate
- Oblate shape
- Inertially axi-symmetrical mass geometry
- Large aspect ratio
- Large nutation angle (i.e., far from major-axis spin)

Clearly, many aspects of the capture problem are not reflected in the current simulation model. Some of the topics to be addressed in future work include the following:

- *Design realizability*. Although the design optimization was carried out with realistic bounds on stiffness and damping parameters, the parameters for each degree of freedom were chosen independently. For a given passive mechanical system, additional constraints will inevitably exist between the various degrees of freedom; these can be taken into account by introducing additional constraints in the optimization problem.
- *Precision of angular velocity match*. For the results in Section 8, it was assumed that the capture mechanism attaches to the asteroid instantaneously, at the moment when the angular velocity of the spacecraft is precisely matched with that of the asteroid. In reality, the capture will not be instantaneous, and there will be some residual relative motion between the asteroid and the spacecraft.
- *Settling dynamics*. In addition to the loads caused by the

motion of the asteroid, the act of quicly grabbing an unevenly shaped asteroid will induce loads on the spacecraft at the very beginning of the grapple phase

We end by noting that hardware-in-the-loop simulations, incorporating a scale model of an actual capture device, are planned for the future.

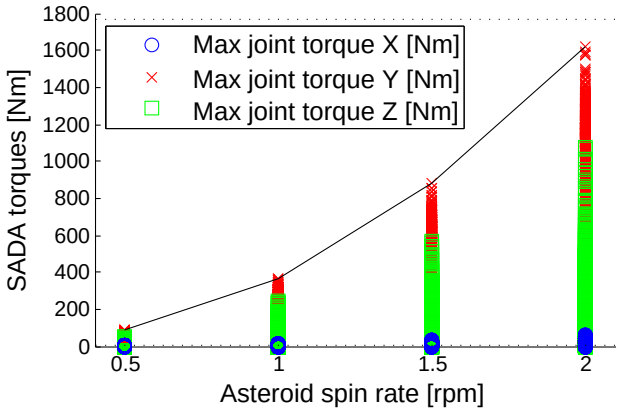

(a) SADA joint torques

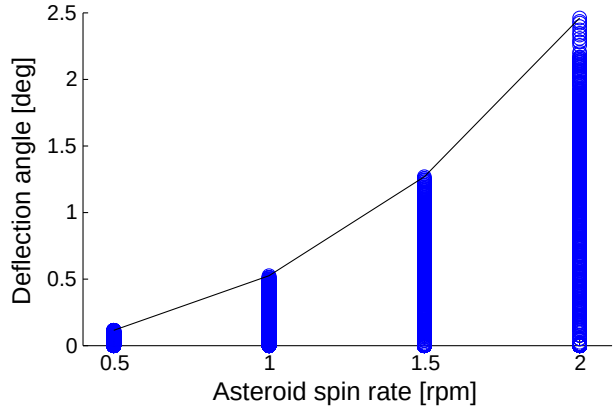

(b) Deflection angle

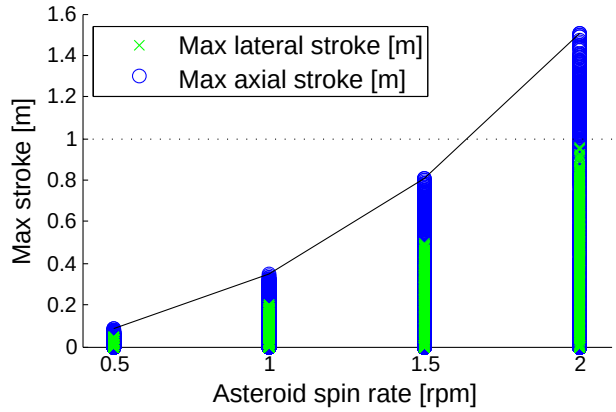

(c) Lateral and axial strokes

Figure 19. Parametric sweep results. The black lines show the maximum value at each spin rate.

ACKNOWLEDGMENTS

The research described in this paper was carried out at the Jet Propulsion Laboratory, California Institute of Technology, under a contract with the National Aeronautics and Space Administration.

We would like to thank the members of the capture mechanism design and GN&C teams, with special thanks to Brian Wilcox (capture mechanism design lead), A. Miguel San-Martin (GN&C lead), Louis Giersch (soft-goods design/analysis), and Gurkirpal Singh (GN&C algorithms).

REFERENCES

[1] J. Brophy, F. Culick, F. Friedman, et al., "Asteroid retrieval feasibility study," Keck Institute for Space Studies, California Institute of Technology, Tech. Rep., 04 2012.

[2] C. Lim and A. Jain, "Dshell++: A component based, reusable space system simulation framework," in *Proc. Third IEEE International Conference on Space Mission Challenges for Information Technology*, Pasadena, CA, 2009.

[3] P. C. Hughes, *Spacecraft Attitude Dynamics*. Dover, 2004.

[4] J. A. Burns and V. S. Safronov, "Asteroid nutation angles," *Monthly Notices of the Royal Astronomical Society*, vol. 165, pp. 403–411, 1973.

[5] D. E. Goldberg, *Genetic Algorithms in Search, Optimization and Machine Learning*, 1st ed. Boston, MA, USA: Addison-Wesley Longman Publishing Co., Inc., 1989.

[6] A. Chipperfield and P. Fleming, "The MATLAB genetic algorithm toolbox," in *IEE Colloquium on Applied Control Techniques Using MATLAB*, 1995, pp. 10/1–10/4.

[7] A. Fukunaga, S. Chien, D. Mutz, R. Sherwood, and A. Stechert, "Automating the process of optimization in spacecraft design," in *Proc. IEEE Aerospace Conference*, vol. 4, 1997, pp. 411–427.

[8] J. Lohn, D. Linden, G. Hornby, and W. Kraus, "Evolutionary design of an X-band antenna for NASA's space technology 5 mission," in *Proc. IEEE Antenna and Propagation Society International Symposium*, vol. 3, 2004, pp. 2313–2316.

[9] T. Mosher, "Conceptual spacecraft design using a genetic algorithm trade selection process," *Journal of Aircraft*, vol. 36, no. 1, pp. 200–208, 1999.